

A Swash Mass Unmanned Aerial Vehicle: Design, Modeling and Control

Andrea M. Tonello and Babak Salamat

Abstract—In this paper, a new unmanned aerial vehicle (UAV) structure, referred to as swash mass UAV, is presented. It consists of a double blade coaxial shaft rotor and four swash masses that allow changing the orientation and maneuvering the UAV. The dynamical system model is derived from the Newton's law framework. The rotational behavior of the UAV is discussed as a function of the design parameters. Given the uniqueness and the form of the obtained non-linear dynamical system model, a back-stepping control mechanism is proposed. It is obtained following the Lyapunov's control approach in each iteration step. Numerical results show that the swashed mass UAV can be maneuvered with the proposed control algorithm so that linear and aggressive trajectories can be accurately tracked.

Index Terms—Aerospace, Unmanned aerial vehicle, dynamical system model, non-linear control, back-stepping control, trajectory tracking.

I. INTRODUCTION

OVER the past few decades unmanned aerial vehicles (UAVs) have received growing attention for their versatility in different application domains. Initially conceived for military applications, nowadays they find deployment in surveillance systems, aerial photography, traffic control, and agriculture. In addition, their navigation autonomy, compact size, low environmental impact when electrically propelled, drive the development of new commercial business models for logistics, e.g., parcel delivery, and future urban transportation services, e.g., aerial taxi. To fulfill the diverse requirements of the cited applications, the design of new mechanical structures is a quite vivid research activity. Such structures, essentially, can be divided into three significant categories: fixed-wing (FW) UAVs, rotary-wing (RE) UAVs and hybrid-layout (HL) UAVs [1]. The fixed-wing UAVs have fixed-wings appropriately shaped and positioned to produce lift from the forward movement of the vehicle. FW UAVs reach high-speeds and have the ability to fly over long distances. However, they require horizontal take-off and landing procedures. On the other hand, rotary-wing UAVs offer vertical take-off and landing capabilities as well as the ability to hover in a motionless spot. Quadrotor helicopters are a popular example of RW UAVs. The rotor disks are aligned in a single plate and the quadrotor's thrust vector is constrained vertically to the plate. Indeed, rotary-wing UAVs are not aerodynamically optimized as fixed-wing UAVs and reach lower speeds and flight distance. To increase their limited maneuverability [2],

Andrea M. Tonello is with the Alpen-Adria-Universität Klagenfurt, Institute of Networked and Embedded Systems, 9020, Austria, e-mail: andrea.tonello@aau.at.

Babak Salamat is with the Alpen-Adria-Universität Klagenfurt, Institute of Networked and Embedded Systems, 9020, Austria, e-mail: babaksa@edu.aau.at.

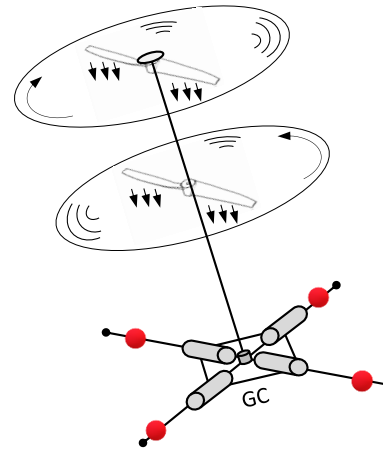


Fig. 1: Swash mass unmanned aerial vehicle structure.

[3], a number of modified configurations have been developed. For instance, the authors in [4], [5], [6] propose a multi-rotor helicopter with the ability to tilt the propellers so that the thrust vector direction can be changed. To combine the advantages of both FW and RW UAVs, hybrid-layout UAVs have been conceived and they deploy both wings and thrust rotors. However, they are mechanically complex due to the rotor inclination apparatus [7]. In all UAV systems, a key component is the automatic control mechanism. Different control methodologies have been studied for the trajectory tracking problem. A linear quadratic regulator (LQR) approach has been considered in [8], [9], [10] for trajectory tracking of a quadrotor UAV in the presence of external disturbances. Bounded tracking control was analyzed in [11] for a wide class of reference trajectories. Stochastic feedback control was proposed for a fixed-wing UAV in [12], [13]. Interconnection and damping assignment passivity based control (IDA-PBC) has been applied in [14], [15] for the vertical takeoff and landing of a degree one under actuated aircraft with strong input coupling. Finally, since the dynamical system model is often nonlinear and with a number of coupled subsystems, non-linear back-stepping control mechanisms have been considered valuable. For instance, Lyapunov based back-stepping control has been investigated for position tracking of a quadrotor UAV in [16], [17].

In this paper, the main contribution is twofold. We first propose and model a novel unmanned aerial vehicle structure (Fig. 1). Then, we address the control mechanism for trajectory tracking. In reference to the UAV structure, the basic idea is

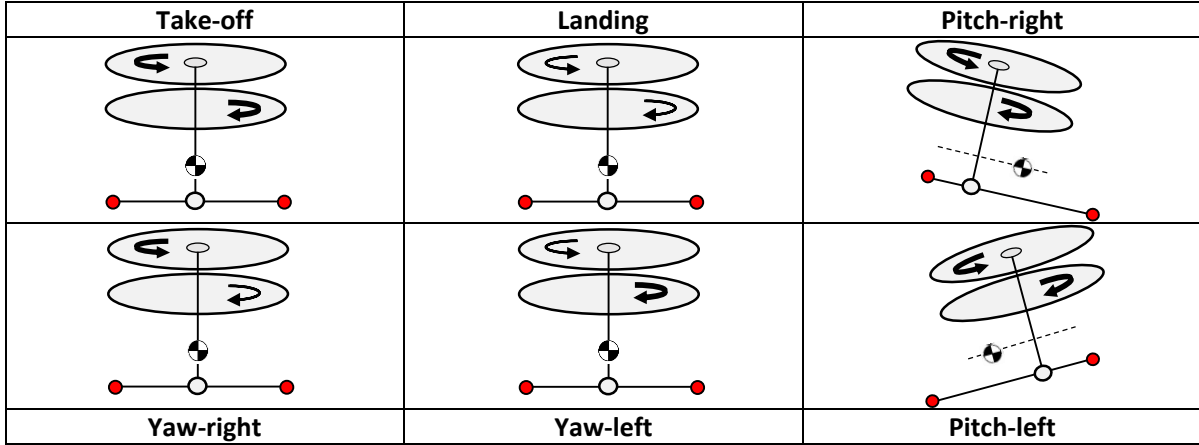


Fig. 2: Take-off, landing and yaw motion of the swash mass UAV.

to deploy a double blade coaxial shaft rotor and to maneuver the helicopter through the linear movement of four masses positioned on the main body plate. We refer to it as the swashed mass helicopter. The rotors provide a drag thrust, while the inertial masses (through the gravitational forces) induce a certain orientation so that to attain a certain roll, pitch and yaw. By controlling the rotors speed and the swash masses displacement it is possible (as it will be shown) to control the UAV to follow certain trajectories, as well as to provide VTOL and hovering ability. In contrast, traditional helicopters, for instance those with body and tail rotor wings, deploy a collective pitch swash-plate [18] that is capable to change the main blade pitch angle, and then they adapt the main and tail blade speeds to induce certain maneuvers. However, the swash plate mechanisms is mechanically complex and of difficult realization in small UAVs.

In more detail, the specific contributions of this paper are:

- the description of the swash mass helicopter structure;
- the derivation of the dynamical system model;
- the effect of sizing on control input response;
- the development of a control strategy using a non linear back-stepping control methodology ([19], Chapter 2) to both stabilize the rotor craft and track a certain trajectory.

The derived back-stepping control mechanism nicely applies to the proposed novel UAV structure since the dynamic system model can be divided into a fully actuated subsystem and a coupled underacted subsystem. Furthermore, the dynamical system model includes the derivative of the control inputs, as a result of a time variant inertia matrix, which makes the control design challenging. To overcome this challenge and derive the control law, we propose a simplified state space dynamic model by approximating the inertia matrix with a constant value.

The reminder of this paper is organized as follows. The basic characteristics of the UAV structure are given in Section II. The mathematical formulation of the system dynamics is presented in Section III. The equilibrium analysis as well as design guidelines (sizing) of the structure are given in Section IV. The control problem is addressed in Section V. Several simulation results are presented in Section VI. The conclusions

then follow.

Notation: Vectors and matrices are denoted with bold letters. Unless stated otherwise, all vectors in this paper are column vectors. The vector cross product is denoted with \times . The state variables are a function of time, e.g., $\mathbf{x} = \mathbf{x}(t)$. The first and second derivative with respect to time of a state space variable x are denoted respectively with \dot{x} , and \ddot{x} .

II. BASIC ELEMENTS OF THE SWASH MASS UAV

The proposed UAV deploys a coaxial double blade rotor with the rotor connected to the main helicopter body via a rigid shaft. To steer the helicopter, four masses are displaced on an orthogonal plane w.r.t. to the rotor shaft and can moved with linear cross shaft servos. Assuming the rotor and blades to be concentrated in one point in the rotor shaft edge, we refer to such a point as the rotor center (RC). The intersection of the rotor shaft and the swash masses plane is referred to as geometrical center (GC) of the UAV. The blades rotation induces a thrust aligned with the rotor shaft and the swash masses shifts the center of mass (CM) of the UAV on an orthogonal plane to the thrust vector, i.e., it tilts the UAV body (Fig. 2). A yaw movement is generated by changing the relative speed of the two blades since a drag torque imbalance is generated, while roll and pitch are regulated by displacing the swash masses asymmetrically w.r.t. the GC.

III. DYNAMICAL SYSTEM MODEL

In this section, firstly, the coordinate systems will be defined. Then, the full non-linear dynamical system model describing the UAV's translation and rotation will be derived using the Newton's framework.

A. Coordinate Systems

To describe the behaviour (translation and rotation) of the UAV, three coordinate systems can be defined: the inertial reference frame, the center of mass (CM) frame aligned with the inertial reference frame and attached to the CM and the

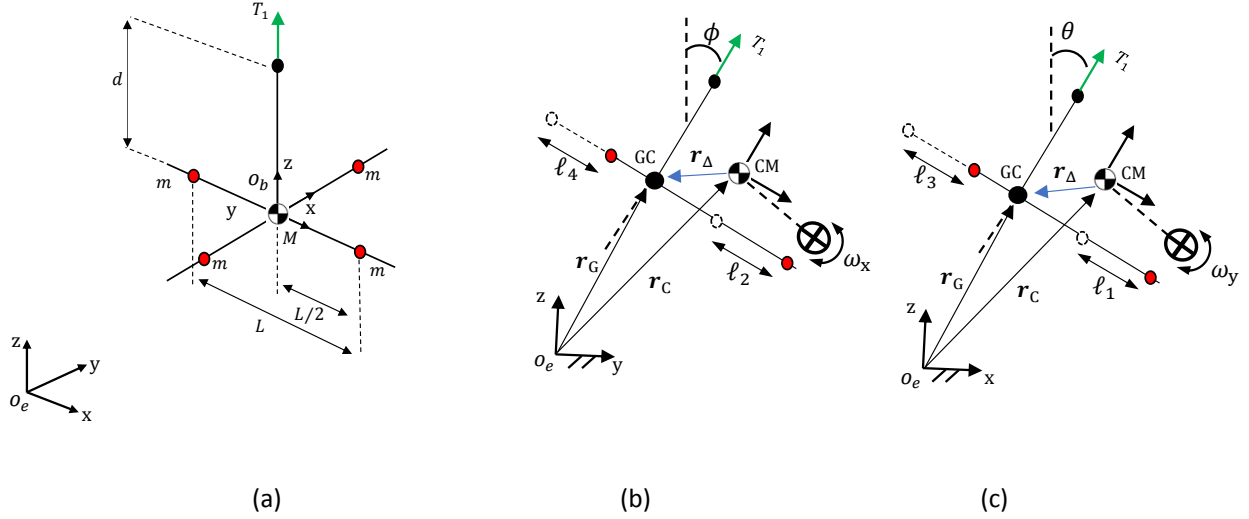


Fig. 3: Free diagram of the swash mass UAV. (a) Reference frames O_e and O_b . The connection between the frames is denoted with radius vectors \mathbf{r}_G , \mathbf{r}_c and \mathbf{r}_Δ . (b) The planner UAV equipped with two swash masses in $y-z$ plane. Main body (GC), swash masses $2m$ and the center of mass (CM). Showing only pitch dynamics for clarity. (c) The planner UAV equipped with two swash masses in $x-z$ plane.

body-fixed reference frame. Note that we express angular momentum and angular velocities w.r.t. the CM frame.

The body-fixed reference frame $O_b = \{x_b, y_b, z_b\}$ is centered in the GC (see Fig. 3). The z_b axis has the orientation of the rotor shaft and it is orthogonal to the swash masses plane. The two mass cross shafts are aligned with the x_b and y_b axes.

The inertial reference frame is $O_e = \{x, y, z\}$ and it is fixed on the earth ground with the gravity vector pointing towards the negative z direction¹.

We also use the following notation for radius and velocity vectors: \mathbf{r}_c denotes radius vector from the inertial reference frame O_e to the CM frame while $(\mathbf{r}_\Delta)_b$ denotes the radius vector from the CM frame to the body-fixed reference frame O_b expressed in the body-fixed reference frame. \mathbf{r}_G denotes the radius vector from the inertial reference frame O_e to the GC of the UAV.

Since the body reference frame is fixed to the unmanned aerial vehicle structure, it translates and rotates with the body [21]. Its rotation w.r.t. the CM frame is given by the Euler angles (ϕ, θ, ψ) .

Finally, we can relate the body-fixed reference frame to the inertial reference frame by the rotation matrix \mathbf{R}_B^I which passes a vector from the former frame to the latter [20]. Its rotation w.r.t. the inertial reference frame (shifted so that it has the same origin of the body reference frame) is given by the rotation matrix

$$\mathbf{R}_B^I = \begin{bmatrix} c_\theta c_\psi & s_\phi s_\theta c_\psi - c_\phi s_\psi & c_\phi s_\theta c_\psi + s_\phi s_\psi \\ c_\theta s_\psi & s_\phi s_\theta s_\psi - c_\phi c_\psi & c_\phi s_\theta s_\psi - s_\phi c_\psi \\ -s_\theta & s_\phi c_\theta & c_\phi c_\theta \end{bmatrix}. \quad (1)$$

The terms s . and c . represent the sine and cosine functions of the argument in the subscript, respectively.

¹We assume that the Earth-fixed frame can be considered as an inertial reference frame since the effect of Earth's rotation on an aerial object moving from the North pole towards the equator can be neglected [20].

B. External Forces and Moments

We assume that the UAV has a mass M , including the four swash masses each with identical value m , which is concentrated in the CM of the UAV. The UAV is subjected to translational and rotational forces in a constant gravitational field with the gravity \mathbf{g} that is aligned to the inertial reference frame z -axis. Therefore, the overall gravitational force expressed in the inertial reference frame can be written as follows

$$\mathbf{F}_{g,I} = \begin{bmatrix} 0 \\ 0 \\ -Mg \end{bmatrix}. \quad (2)$$

The thrust is the main force generated by the rotation of the two blades. Overall, the net thrust T_1 (which is aligned with the rotor shaft) can be written in the shifted inertial reference frame (with origin RC) as follows

$$\mathbf{F}_{r,I} = \mathbf{R}_B^I \mathbf{F}_{r,B} = \mathbf{R}_B^I \begin{bmatrix} 0 \\ 0 \\ T_1 \end{bmatrix}, \quad (3)$$

where T_1 (which is directly proportional to the upper and lower rotor aerodynamic coefficient γ_1 and to the rotational speeds Ω_1 and Ω_2 [18]) equals $T_1 = \gamma_1(\Omega_1^2 + \Omega_2^2)$.

The UAV is tilted by steering the swash masses since they generate a moment vector about an axis passing through the CM. Such a moment vector can be expressed in the shifted inertial frame (CM frame) as follows

$$\begin{aligned} \mathbf{M}_C &= \mathbf{R}_B^I (\mathbf{r}_\Delta)_b \times \mathbf{R}_B^I \begin{bmatrix} 0 \\ 0 \\ T_1 \end{bmatrix} + \mathbf{R}_B^I \begin{bmatrix} 0 \\ 0 \\ \gamma_2(\Omega_1^2 - \Omega_2^2) \end{bmatrix} \\ &= \mathbf{R}_B^I \left((\mathbf{r}_\Delta)_b \times \begin{bmatrix} 0 \\ 0 \\ T_1 \end{bmatrix} \right) + \mathbf{R}_B^I \begin{bmatrix} 0 \\ 0 \\ \gamma_2(\Omega_1^2 - \Omega_2^2) \end{bmatrix}. \end{aligned} \quad (4)$$

The yaw moment $M_\psi = \gamma_2(\Omega_1^2 - \Omega_2^2)$ generated by the rotating blades is directly proportional to the corresponding aerodynamic coefficient γ_2 and rotation speeds difference [18].

C. Complete Non-linear Dynamical System Model

The translational dynamics of the CM w.r.t. the inertial reference frame can be obtained by applying the first cardinal Newton's equation [20], [22] and exploiting (2) and (3). The model becomes:

$$\begin{bmatrix} \ddot{x} \\ \ddot{y} \\ \ddot{z} \end{bmatrix}_C = \frac{1}{M} \mathbf{F}_{g,I} + \frac{1}{M} \mathbf{F}_{r,I}. \quad (5)$$

Our objective is to derive the translational dynamics of the geometric center (GC) of the helicopter observed in the inertial reference frame. To do so, we consider a shift (see Fig. 3 (b-c)), and write

$$\mathbf{r}_G = \mathbf{r}_C + \mathbf{r}_\Delta. \quad (6)$$

We use the fact that $\mathbf{r}_\Delta = \mathbf{R}'_B(\mathbf{r}_\Delta)_b$, where \mathbf{R}'_B and $(\mathbf{r}_\Delta)_b$ are the rotation matrix from the body-fixed frame to the CM frame and the radius vector from the CM frame to the body-fixed reference frame expressed in the body-fixed frame, respectively. Taking the time derivative of both sides of (6) and using the identity $\dot{\mathbf{R}}'_B(\mathbf{r}_\Delta)_b = \mathbf{R}'_B(\boldsymbol{\omega} \times (\dot{\mathbf{r}}_\Delta)_b)$ [23], we get

$$\dot{\mathbf{r}}_\Delta = \mathbf{R}'_B \left[(\dot{\mathbf{r}}_\Delta)_b + \boldsymbol{\omega} \times (\mathbf{r}_\Delta)_b \right], \quad (7)$$

where $\boldsymbol{\omega} = [\omega_x \ \omega_y \ \omega_z]^T$ is the angular velocity vector. Taking one more time derivative we obtain

$$\ddot{\mathbf{r}}_\Delta = \mathbf{R}'_B \left[(\ddot{\mathbf{r}}_\Delta)_b + 2\boldsymbol{\omega} \times (\dot{\mathbf{r}}_\Delta)_b + \dot{\boldsymbol{\omega}} \times (\mathbf{r}_\Delta)_b + \boldsymbol{\omega} \times (\boldsymbol{\omega} \times (\mathbf{r}_\Delta)_b) \right]. \quad (8)$$

Substituting (8) in (6), we obtain the translational dynamics of the GC w.r.t. the inertial reference frame. To make our notation simple, we define

$$\begin{bmatrix} x \\ y \\ z \end{bmatrix}_{GC} \triangleq \begin{bmatrix} x \\ y \\ z \end{bmatrix}. \quad (9)$$

Therefore, we obtain

$$\begin{bmatrix} \ddot{x} \\ \ddot{y} \\ \ddot{z} \end{bmatrix} = \mathbf{R}'_B \left[(\ddot{\mathbf{r}}_\Delta)_b + 2\boldsymbol{\omega} \times (\dot{\mathbf{r}}_\Delta)_b + \dot{\boldsymbol{\omega}} \times (\mathbf{r}_\Delta)_b + \boldsymbol{\omega} \times (\boldsymbol{\omega} \times (\mathbf{r}_\Delta)_b) \right] + \frac{1}{M} \mathbf{F}_{g,I} + \frac{1}{M} \mathbf{F}_{r,I}, \quad (10)$$

where $(\mathbf{r}_\Delta)_b$ can be easily computed as follows:

$$\begin{aligned} (\mathbf{r}_\Delta)_b &= -\frac{\sum_{i=1}^4 m_i \mathbf{r}_{b,i}}{m_b + \sum_{i=1}^4 m_i} = -\frac{\sum_{i=1}^4 m_i \mathbf{r}_{b,i}}{M} \\ &= -\frac{m}{M} \left(\begin{bmatrix} \frac{L}{2} + \ell_1 \\ 0 \\ 0 \end{bmatrix} + \begin{bmatrix} -\frac{L}{2} + \ell_3 \\ 0 \\ 0 \end{bmatrix} + \begin{bmatrix} 0 \\ \frac{L}{2} + \ell_2 \\ 0 \end{bmatrix} \right. \\ &\quad \left. + \begin{bmatrix} 0 \\ -\frac{L}{2} + \ell_4 \\ 0 \end{bmatrix} \right) = -\beta \begin{bmatrix} \ell_1 + \ell_3 \\ \ell_2 + \ell_4 \\ 0 \end{bmatrix}, \end{aligned} \quad (11)$$

where we define β as the ratio of the swash mass weight and the total UAV weight $\beta = \frac{m}{M}$, m_b denotes the mass of the UAV rigid body (without steering masses), $\mathbf{r}_{b,i}$ represents the position of the i -th swash masses, expressed in the body-fixed frame². $\frac{L}{2}$ and ℓ_i denote the rest position of the i -th swash masses during hovering and the instantaneous position of the i -th swash mass, respectively.

We now determine the angular momentum of our UAV about the center of mass CM, which may have an acceleration $\mathbf{a}_c = [\ddot{x}, \ddot{y}, \ddot{z}]_c^T$. The rotational motion can be obtained by applying the second cardinal Newton's equation (Euler's moment equation) [22] as follows

$$\left(\frac{d\mathbf{L}}{dt} \right)_C = \mathbf{M}_C. \quad (12)$$

The angular momentum \mathbf{L} is equal to

$$\mathbf{L} = \sum_{i=1}^5 \mathbf{r}_i \times \mathbf{Q}_i = \sum_{i=1}^5 \mathbf{r}_i \times m_i \mathbf{v}_i = \sum_{i=1}^5 \mathbf{r}_i \times (\boldsymbol{\omega} \times \mathbf{r}_i) m_i = \mathbf{I} \boldsymbol{\omega}, \quad (13)$$

where \mathbf{r}_i is the position vector relative to the CM of the representative particle of mass m_i , $m_i = m$ for $i = 1, \dots, 4$ and $m_5 = m_b$. For our system, the velocity of m_i relative to CM is $\dot{\mathbf{r}}_i = \boldsymbol{\omega} \times \mathbf{r}_i$. $\mathbf{I} \in \mathbb{R}^{3 \times 3}$ is the overall inertia tensor, or inertia matrix of the system. In computing the angular momentum \mathbf{L} it should be taken into account the fact that, due to the swash masses, the inertia matrix is time-dependent. Furthermore, we assume the two swash masses to be mutually constrained at constant distance L and $\frac{L}{2} + \ell_2 - (-\frac{L}{2} + \ell_4) = L$ and $\frac{L}{2} + \ell_1 - (-\frac{L}{2} + \ell_3) = L$. Since, $\ell_2 = \ell_4$ and $\ell_1 = \ell_3$, for simplicity we define $\ell_y = 2\ell_2$ and $\ell_x = 2\ell_1$. The elements of the inertia matrix can be computed as follows

$$\begin{aligned} I_{xx} &= m_b \left[-2\beta \ell_y \right]^2 \\ &+ m \left[\left(\frac{1}{2} - 2\beta \right) \ell_y + \frac{L}{2} \right]^2 + m \left[\left(\frac{1}{2} - 2\beta \right) \ell_y - \frac{L}{2} \right]^2 \end{aligned} \quad (14)$$

$$\begin{aligned} I_{yy} &= m_b \left[-2\beta \ell_x \right]^2 \\ &+ m \left[\left(\frac{1}{2} - 2\beta \right) \ell_x + \frac{L}{2} \right]^2 + m \left[\left(\frac{1}{2} - 2\beta \right) \ell_x - \frac{L}{2} \right]^2 \end{aligned} \quad (15)$$

²Note that we assume that the origin of the GC coincides with the CM of the UAV during hovering.

$$\begin{aligned}
I_{zz} &= m_b \left[-2\beta\ell_y \right]^2 + m_b \left[-2\beta\ell_x \right]^2 \\
&+ m \left[\left(\frac{1}{2} - 2\beta \right) \ell_x + \frac{L}{2} \right]^2 + m \left[\left(\frac{1}{2} - 2\beta \right) \ell_x - \frac{L}{2} \right]^2 \\
&+ m \left[\left(\frac{1}{2} - 2\beta \right) \ell_y + \frac{L}{2} \right]^2 + m \left[\left(\frac{1}{2} - 2\beta \right) \ell_y - \frac{L}{2} \right]^2 \\
I_{xy} = I_{yx} &= -m_b \left[\begin{bmatrix} -2\beta\ell_y \cos(\phi) \\ -2\beta\ell_x \cos(\theta) \end{bmatrix} \begin{bmatrix} -2\beta\ell_x \cos(\theta) \\ -2\beta\ell_y \cos(\phi) \end{bmatrix} \right] \\
&- m \left[\left[\left(\frac{1}{2} - 2\beta \right) \ell_x \cos(\theta) + \frac{L}{2} \cos(\theta) \right] \right. \\
&\left. \left[\left(\frac{1}{2} - 2\beta \right) \ell_y \cos(\phi) + \frac{L}{2} \cos(\phi) \right] \right] \\
&- m \left[\left[\left(\frac{1}{2} - 2\beta \right) \ell_x \cos(\theta) - \frac{L}{2} \cos(\theta) \right] \right. \\
&\left. \left[\left(\frac{1}{2} - 2\beta \right) \ell_y \cos(\phi) - \frac{L}{2} \cos(\phi) \right] \right] \\
I_{xz} = I_{yz} &= 0.
\end{aligned} \tag{16}$$

We are in the position to write the full dynamical system model.

Full Swash Mass UAV Dynamical System Model: From the results above, the full non-linear dynamical system model of the UAV can be written as

$$\begin{bmatrix} \ddot{x} \\ \ddot{y} \\ \ddot{z} \end{bmatrix} = \mathbf{R}_B^I \left[\begin{bmatrix} \ddot{\mathbf{r}}_{\Delta} \end{bmatrix}_b + 2\boldsymbol{\omega} \times \begin{bmatrix} \dot{\mathbf{r}}_{\Delta} \end{bmatrix}_b + \dot{\boldsymbol{\omega}} \times \begin{bmatrix} \mathbf{r}_{\Delta} \end{bmatrix}_b \right. \\
\left. + \boldsymbol{\omega} \times \left(\boldsymbol{\omega} \times \begin{bmatrix} \mathbf{r}_{\Delta} \end{bmatrix}_b \right) \right] + \frac{1}{M} \mathbf{F}_{g,I} + \frac{1}{M} \mathbf{F}_{r,I}, \tag{18}$$

$$\dot{\boldsymbol{\omega}} + \mathbf{I} \boldsymbol{\omega} = \mathbf{M}_C. \tag{19}$$

Remark 1. The model has six outputs $\{x, y, z, \phi, \theta, \psi\}$ and only four control inputs $\{T_1, \ell_y, \ell_x, M_\psi\}$. Therefore, the UAV is an under-actuated dynamical system. Furthermore, it should be noted that such a dynamical system is not common since the inertia matrix depends on the control inputs which in turn make it time dependent. This is taken into account in the relation (19).

IV. EFFECT OF SIZING ON CONTROL INPUT RESPONSE

In this section, we want to get an understanding of the motion behavior of the considered UAV. This helps the dimensioning/sizing of its structure as a function of the design parameters, and to introduce the control problem (discussed in the next section). We start by analyzing the effect of sizing on the control input response.

For the sake of exposition simplicity, to analyze the effect of sizing on control input response, we assume a 2D planner

scenario so that the UAV structure can be depicted as in (Fig. 3 (b)). The planner dynamics, obtained from (18) and (19), then becomes as follows

2D Dynamical System Model: If we consider a two dimensions UAV structure, the dynamical system model reads as follows

$$\begin{aligned}
\mathbf{M} \begin{bmatrix} \ddot{y} \\ \ddot{z} \end{bmatrix} &= \beta \begin{bmatrix} 2\dot{\phi}\dot{\ell}_y \sin(\phi) - \ddot{\ell}_y \cos(\phi) + \ell_y \ddot{\phi} \sin(\phi) + \ell_y \dot{\phi}^2 \cos(\phi) \\ -\ddot{\ell}_y \sin(\phi) + \ell_y \dot{\phi}^2 \sin(\phi) - 2\dot{\phi}\dot{\ell}_y \cos(\phi) - \ell_y \ddot{\phi} \cos(\phi) \end{bmatrix} \\
&+ \begin{bmatrix} T_1 \sin(\phi) \\ T_1 \cos(\phi) \end{bmatrix} - \begin{bmatrix} 0 \\ Mg \end{bmatrix} \\
&\left[m_b (-2\beta\ell_y)^2 + m \left(\left(\frac{1}{2} - 2\beta \right) \ell_y + \frac{L}{2} \right)^2 \right. \\
&\left. + m \left(\left(\frac{1}{2} - 2\beta \right) \ell_y + \frac{L}{2} \right)^2 \right] \ddot{\phi} \\
&+ \left[\ell_y \dot{\ell}_y (m - 8\beta m + 16\beta^2 m + 8\beta^2 m_b) \right] \dot{\phi} = \beta T_1 \cos(\phi) \ell_y.
\end{aligned} \tag{20}$$

In this case, the control inputs are limited to $\mathbf{u} = [T_1, \ell_y]^T$. While the angle ϕ in (21) is determined only by the UAV main design parameters M, m, L , the swash mass position ℓ_y and the thrust T_1 , the translational motion in (20) depends on the thrust T_1 , swash mass position ℓ_y , velocity $\dot{\ell}_y$, acceleration $\ddot{\ell}_y$ and the pitch angle ϕ . Since, only the rotational dynamics in (21) is of importance at this point, we set the thrust around the hovering point, which is $T_1 = \frac{Mg}{\cos(\phi)}$. We analyse the rotational dynamics in (21) for an elementary control input as a function of design parameters M, m, L . We consider the control input ℓ_y to be equal to a saw triangle function as shown in Fig. 4 (a). In Fig. 4, we plot the relation between:

- the control input ℓ_y ;
- the pitch angle response and the arm length L for a given constant mass ratio $\beta = \frac{m}{M}$;
- the pitch angle response and the mass ratio $\beta = \frac{m}{M}$ for a given constant L .

Fig. 4 (b) shows that it is sufficient to have the arm length L equal $0.4m$ for a given constant mass ratio $\beta = \frac{m}{M} = 0.09$ to induce a high value for the pitch angle response. The pitch response increases sharply for a given constant $L = 0.3m$ (Fig. 4 (c)) as the mass ratio $\beta = \frac{m}{M}$ increases. From the results, it can be seen that the pitch angle ϕ reaches a maximum value ϕ_{max} . Therefore, in Fig. 5 we plot the maximum value of pitch angle ϕ_{max} as a function of the pair made of the arm length L and the mass ratio $\beta = \frac{m}{M}$. Overall, it can be seen that there exist several design solutions, i.e., choices of the parameters M, m, L , to have the UAV reach a given pitch angle.

The presented results suggest that to obtain better dynamical performance, one should increase $\beta = \frac{m}{M}$ indefinitely. In practice, the swash mass weight is limited due to the physical constraint of the UAV's structure and we can not distribute all the weight on the swash masses only. Therefore, the design strategy is to provide a trade-off between the design parameters of the UAV and the mission flight requirements.

An example of design parameters that will be used also in the numerical results section, is reported in Table I.

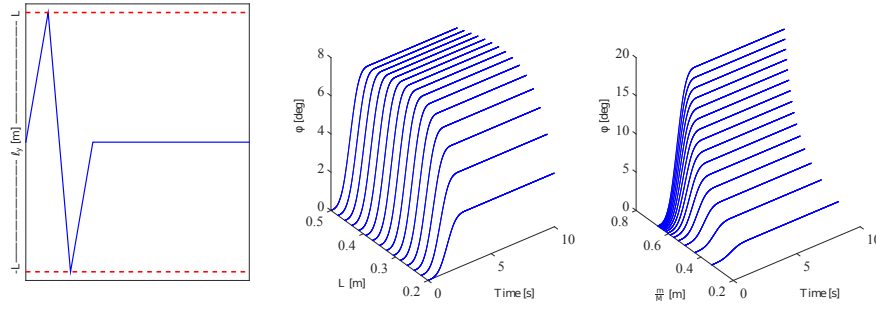


Fig. 4: Effect of sizing on control input response. a) a saw triangle function ℓ_y . b) Relation between the pitch angle ϕ and the arm length L for a given constant mass ratio $\beta = \frac{m}{M} = 0.09$. c) Relation between the pitch angle ϕ and the mass ratio $\beta = \frac{m}{M}$ for a given constant $L = 0.3m$.

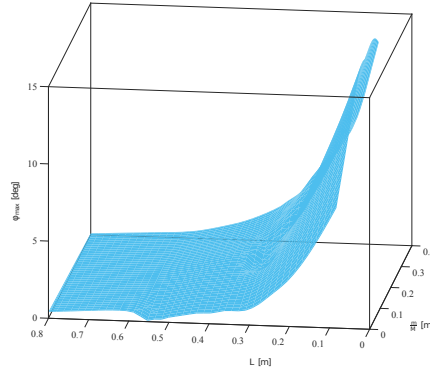


Fig. 5: Maximum pitch angle ϕ_{max} as a function of the mass ratio β and arm length L .

In the next section, we develop a control law that allows the UAV to follow a certain trajectory.

V. TRAJECTORY TRACKING AND CONTROL

The main objective of the automatic control is to act on the rotor thrust and swash masses position so that the UAV can track a desired target trajectory $\{x_*, y_*, z_*\}$ with stable Euler angles. To proceed, for the sake of exposition and understanding simplicity, we focus first on the 2D planner. The derivation of the control laws in the full 3D case, will be given next (Section V).

In the 2D planner, we can make two observations: firstly, the dynamical system comprises two main sub-systems (altitude and horizontal coordinate relations in (20) that are coupled via the control input T_1 and the pitch angle ϕ), and a third sub-system (pitch angle relation (21) with control input ℓ_y coupled to the other subsystems via the pitch angle ϕ itself). The pitch angle is determined by the control input ℓ_y only. Secondly, the dynamics of the pitch angle depends not only on the input ℓ_y but also on its derivative.

The first observation suggests the use of a non-linear back-stepping control mechanism. Back-stepping control is an iterative approach that breaks down the controller design into steps and therefore the control of each sub-system is implemented iteratively [19], [24]. In detail, since we want to control the UAV via T_1 and ℓ_y to follow a certain target trajectory $(y_*(t), z_*(t))$, we first determine the control input T_1 to reach the target altitude. Then, we define the virtual control input $u_y = \sin(\phi)$ and derive a control law for it to reach the target horizontal coordinate. Finally, we regulate the value of

ℓ_y so that the pitch angle ϕ derived from the virtual control input u_y is obtained. Furthermore, each control law in the back-stepping process is derived via the Lyapunov methodology [25].

The second observation suggests to proceed by deriving a dynamical system model where the inertia term in (21) is approximated with an appropriate constant value. In particular, since the inertia term varies as the swash masses move from a minimum to a maximum displacement position, we propose to approximate it as

$$I_{xx} \approx I_c = m_b \left(-2\beta \ell_{mean} \right)^2 + m \left[\left(\frac{1}{2} - 2\beta \right) \ell_{mean} + \frac{L}{2} \right]^2 + m \left[\left(\frac{1}{2} - 2\beta \right) \ell_{mean} - \frac{L}{2} \right]^2, \quad (22)$$

with

$$\ell_{mean} = \left(\frac{\ell_{max} + \ell_{min}}{2} \right). \quad (23)$$

and

$$\ell_{max} = L, \quad \ell_{min} = -L. \quad (24)$$

Therefore, the simplified dynamical system in (21) becomes as follows.

2D Simplified Dynamical System Model: Under the assumption in (22), the 2D dynamical system model reads as follows

$$M\ddot{y} = \beta f_1(\phi, \dot{\phi}, \ell_y, \dot{\ell}_y, \ddot{\ell}_y) + T_1 \sin(\phi) \quad (25)$$

$$M\ddot{z} = \beta f_2(\phi, \dot{\phi}, \ell_y, \dot{\ell}_y, \ddot{\ell}_y) - Mg + T_1 \cos(\phi) \quad (26)$$

$$I_c \ddot{\phi} = \beta T_1 \cos(\phi) \ell_y \quad (27)$$

$$s.t. \quad -L \leq \ell_y \leq L. \quad (28)$$

where

$$f_1(\phi, \dot{\phi}, \ell_y, \dot{\ell}_y, \ddot{\ell}_y) = 2\dot{\phi}\dot{\ell}_y \sin(\phi) - \ddot{\ell}_y \cos(\phi) + \ell_y \ddot{\phi} \sin(\phi) + \ell_y \dot{\phi}^2 \cos(\phi) \quad (29)$$

and

$$f_2(\phi, \dot{\phi}, \ell_y, \dot{\ell}_y, \ddot{\ell}_y) = -\ddot{\ell}_y \sin(\phi) + \ell_y \dot{\phi}^2 \sin(\phi) - 2\dot{\phi}\dot{\ell}_y \cos(\phi) - \ell_y \ddot{\phi} \cos(\phi). \quad (30)$$

Before applying the backstepping approach, we need to be sure that two functions f_1 and f_2 in (25) and (26) are bounded.

Proposition 1. *Let $f_1(\phi, \dot{\phi}, \ell_y, \dot{\ell}_y, \ddot{\ell}_y) = 2\dot{\phi}\dot{\ell}_y \sin(\phi) - \ddot{\ell}_y \cos(\phi) + \ell_y \ddot{\phi} \sin(\phi) + \ell_y \dot{\phi}^2 \cos(\phi)$ be a function defined over a set \mathcal{X} , where all the variables $\phi, \dot{\phi}, \ell_y, \dot{\ell}_y, \ddot{\ell}_y$ in the set \mathcal{X} are bounded. Then, there exists a positive constant Θ_1 such that*

$$\begin{aligned} f_1(\phi, \dot{\phi}, \ell_y, \dot{\ell}_y, \ddot{\ell}_y) &\leq \sqrt{\ddot{\ell}_y^2 + 4\dot{\phi}^2 \ell_y^2} + \sqrt{\ell_y^2 \dot{\phi}^4 + \ell_y^2 \ddot{\phi}^2} \leq \Theta_1 \\ f_1(\phi, \dot{\phi}, \ell_y, \dot{\ell}_y, \ddot{\ell}_y) &\geq -\sqrt{\ddot{\ell}_y^2 + \dot{\phi}^2 \ell_y^2} - \sqrt{\ell_y^2 \dot{\phi}^4 + \ell_y^2 \ddot{\phi}^2} \geq -\Theta_1 \end{aligned} \quad (31)$$

Proof. $f_1(\phi, \dot{\phi}, \ell_y, \dot{\ell}_y, \ddot{\ell}_y) = 2\dot{\phi}\dot{\ell}_y \sin(\phi) - \ddot{\ell}_y \cos(\phi) + \ell_y \ddot{\phi} \sin(\phi) + \ell_y \dot{\phi}^2 \cos(\phi) = a \cos(\phi) + b \sin(\phi) + c \cos(\phi) + d \sin(\phi)$ where $a = -\ddot{\ell}_y$, $b = 2\dot{\phi}\dot{\ell}_y$, $c = \ell_y \dot{\phi}^2$ and $d = \ell_y \ddot{\phi}$. Exploiting the trigonometric property, $f_1(\phi, \dot{\phi}, \ell_y, \dot{\ell}_y, \ddot{\ell}_y)$ can be written as:

$$\begin{aligned} f_1(\phi, \dot{\phi}, \ell_y, \dot{\ell}_y, \ddot{\ell}_y) &= \\ a \cos(\phi) + b \sin(\phi) + c \cos(\phi) + d \sin(\phi) &\equiv \\ \sqrt{a^2 + b^2} \cos\left(\phi - \text{atan}\left(\frac{a}{b}\right)\right) + \sqrt{c^2 + d^2} \cos\left(\phi - \text{atan}\left(\frac{c}{d}\right)\right). \end{aligned} \quad (32)$$

Therefore, we can write

$$\begin{aligned} f_1(\phi, \dot{\phi}, \ell_y, \dot{\ell}_y, \ddot{\ell}_y) &\leq \sqrt{\ddot{\ell}_y^2 + 4\dot{\phi}^2 \ell_y^2} + \sqrt{\ell_y^2 \dot{\phi}^4 + \ell_y^2 \ddot{\phi}^2} \leq \Theta_1 \\ &= \sqrt{\ddot{\ell}_{y,max}^2 + 4\dot{\phi}_{max}^2 \ell_{y,max}^2} + \sqrt{\ell_{y,max}^2 \dot{\phi}_{max}^4 + \ell_{y,max}^2 \ddot{\phi}_{max}^2}. \end{aligned} \quad (33)$$

The last inequality in (33) comes from the fact that a, b, c and d are assumed bounded. By symmetry, we can conclude that $-\sqrt{\ddot{\ell}_y^2 + 4\dot{\phi}^2 \ell_y^2} - \sqrt{\ell_y^2 \dot{\phi}^4 + \ell_y^2 \ddot{\phi}^2} \geq -\Theta_1$ is also bounded. ■

The same bounding methodology can be applied to the second function and we obtain $f_2(\phi, \dot{\phi}, \ell_y, \dot{\ell}_y, \ddot{\ell}_y) \leq \sqrt{\ddot{\ell}_y^2 + 4\dot{\phi}^2 \ell_y^2} + \sqrt{\ell_y^2 \dot{\phi}^4 + \ell_y^2 \ddot{\phi}^2} \leq \Theta_2$.

Now, let $\mathbf{u} = [T_1, \ell_y]^T$ be the control input vector. The dynamics equations (25)-(28) can be written in a state-space realization form $f(\mathbf{x}, \mathbf{u})$ by defining $\mathbf{x} = [x_1, \dots, x_6]^T$ as the state vector:

$$\begin{bmatrix} x_1 \\ x_2 \end{bmatrix} = \begin{bmatrix} y \\ \dot{y} \end{bmatrix}, \begin{bmatrix} x_3 \\ x_4 \end{bmatrix} = \begin{bmatrix} z \\ \dot{z} \end{bmatrix}, \begin{bmatrix} x_5 \\ x_6 \end{bmatrix} = \begin{bmatrix} \phi \\ \dot{\phi} \end{bmatrix}. \quad (34)$$

Consequently, the dynamical system model of the UAV using the state variables in (34) can be written as

$$\dot{x}_1 = x_2 \quad (35)$$

$$\dot{x}_2 = \frac{\beta \Theta_1 + T_1 \sin(x_5)}{M} \quad (36)$$

$$\dot{x}_3 = x_4 \quad (37)$$

$$\dot{x}_4 = -g + \frac{\beta \Theta_2 + T_1 \cos(x_5)}{M} \quad (38)$$

$$\dot{x}_5 = x_6 \quad (39)$$

$$\dot{x}_6 = \frac{\beta T_1 \cos(x_5) \ell_y}{I_c} \quad (40)$$

TABLE I: Example of design parameters of the UAV

Parameters	Symbol	Value	Unit
Mass	M	1.1	kg
Swash mass	m	0.1	kg
Maximum displacement of the mass	L	0.2	m
Gravitational acceleration	g	9.81	m/s ²

A. Altitude and Horizontal Position Control

The control mechanism for the proposed UAV starts by formulating a control law for T_1 (the total thrust generated by two rotor blades), so that given any initial pitch angle $\phi = x_5$ state, we reach a target altitude. The control law is derived by following the Lyapunov methodology [25] applied to the sub-system (26). It is given by:

$$T_1 = \frac{M}{\cos(x_5)} \left[g - \frac{\beta \Theta_2}{M} + e_3 + \ddot{x}_{3*} + k_3 e_4 - k_3^2 e_3 + k_4 e_4 \right], \quad (41)$$

where k_3 and k_4 are control gains with positive value and the error terms are defined as follows:

$$e_3 = x_{3*} - x_3 \quad (42)$$

$$e_4 = x_{4*} - x_4. \quad (43)$$

Now that we have a solution for T_1 , we proceed by deriving a control law for the virtual control input $u_y = \sin(x_5)$ responsible for the motion y , by using the same methodology. After some calculations the law becomes (see Appendix B)

$$u_y = \frac{M}{T_1} \left[-\frac{\beta \Theta_1}{M} + e_1 + \ddot{x}_{1*} + k_5 e_2 - k_5^2 e_1 + k_6 e_2 \right], \quad (44)$$

where k_5 and k_6 are control gains with positive values. In (44), the error terms are defined as follows:

$$e_1 = x_{1*} - x_1 \quad (45)$$

$$e_2 = x_{2*} - x_2. \quad (46)$$

Remark 2. The function u_y obtained in (44), is not a direct control input. However, it determines the desired pitch angle x_{5*} which will be in turn used as the target pitch angle for the regulator of the swash masses displacement ℓ_y (see Fig. 6).

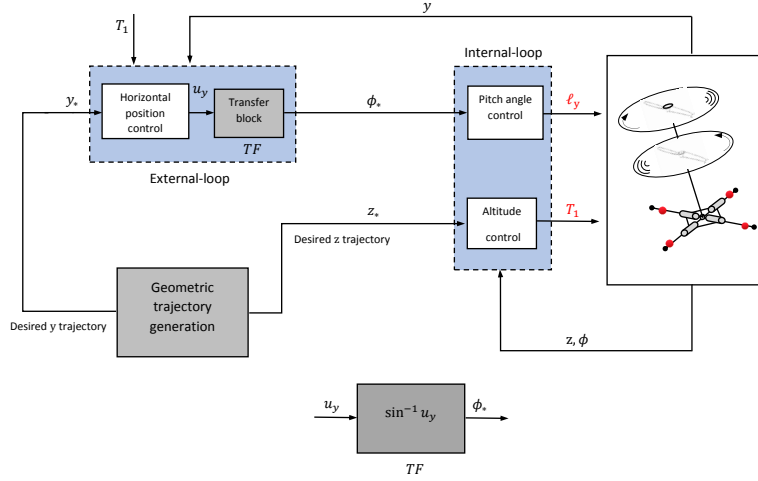


Fig. 6: Back-stepping controller with internal and external control loop architecture, with focus to the 2D case.

Now, the desired pitch angle $x_{5*} = \phi_*$ which is the input to the pitch angle controller, is obtained as:

$$x_{5*} = \sin^{-1}(u_y), \quad (47)$$

where u_y is given by (44). Finally, the desired pitch angle obtained in the above equations serves as the input for the pitch angle controller.

B. Pitch Angle Control

Once we have set the desired pitch angle $x_{5*} = \phi_*$ according to (47), the value of ℓ_y can be regulated via a control law derived by the application of the Lyapunov method as done in the previous sub-sections. The details can be found in the Appendix C and they lead to control law for ℓ_y :

$$\ell_y = \frac{I_c}{\beta T_1 \cos(x_5)} \left[e_5 + k_1 e_6 - k_1^2 e_5 + k_2 e_6 \right], \quad (48)$$

where k_1 and k_2 are control gains with positive value.

Remark 3. The solution ℓ_y in (62) is not necessarily constrained in the range $-L \leq \ell_y \leq L$.

From the *Remark 3*, in order to fulfill the physical constraint for ℓ_y , we propose to introduce a saturation function to obtain

$$\bar{\ell}_y = \text{sat}(\ell_y) = \begin{cases} -L & \ell_y < -L \\ \ell_y & -L < \ell_y < L \\ L & \ell_y > L. \end{cases} \quad (49)$$

However, once the saturation occurs, the errors e_5 and e_6 may increase, which leads to an oscillation of the pitch angle. Therefore, the control law in (62) can be bettered by designing a compensator and modifying the error signals that reduce the influence of the saturation. This leads to the following modified control law

$$\bar{\ell}_{y,m} = \frac{I_c}{\beta T_1 \cos(x_5)} \left[\bar{e}_5 + k_1 \bar{e}_6 - k_1^2 \bar{e}_5 + k_2 \bar{e}_6 \right], \quad (50)$$

where the new error definitions are

$$\bar{e}_5 = e_5 - e^* \quad (51)$$

$$\bar{e}_6 = e_6 - e^*, \quad (52)$$

and the auxiliary error is updated as follows:

$$\dot{e}^* = -\frac{\beta \varepsilon_1}{I_c} e^* + \frac{\beta (\bar{\ell}_{y,m} - \bar{\ell}_y)}{I_c}, \quad (53)$$

with ε_1 being a positive tuning parameter.

Remark 4. It should be observed that instead of saturating ℓ_y , the target pitch angle from (47) can be saturated, i.e., impose a maximum limit to ϕ . However, we found that this provides worse performance.

C. Overall Control Algorithm

The overall back-stepping control algorithm is sketched in Fig. 6. Firstly, the desired trajectories are generated. Feasible trajectories can be obtained for instance, with some waypoints that are located in the search space by the user [26], or they are generated by a stochastic approach [27], [28]. Another approach is using dynamic path planning which the tangent vector field guidance (TVFG) and the Lyapunov vector field guidance (LVFG) are used [29]. From an initial state, the control input T_1 is computed according to (41) to reach a certain altitude. Then, the virtual control input u_y is derived according to (44) to reach a certain horizontal coordinate. This induces a regulation of the pitch angle by setting a target value from (47) and computing the swash masses position ℓ_y according to (50). The procedure is repeated iteratively at each time step to track the target trajectory. It should also be noted that the error terms are computed between the target values and the real UAV state given by the dynamical set of equations (18)-(19). The time step (sampling period) is set to a given small value T_s .

D. Extension to 3D

In this section, we extend the results of the 2D case to derive the control laws for the full 3D system, following the same methodology. Essentially, the control mechanism comprises three steps. The control inputs in the 3D case can be grouped in the control input vector $\mathbf{u} = [T_1, \ell_y, \ell_x, M_\psi]^T$.

Observing (19), we can say that the rotational dynamics is highly coupled. To decouple the three second-order sub-systems of the UAV in (19), we choose the globally defined change of input [30]

$$\begin{bmatrix} \beta T_1 \ell_y \\ \beta T_1 \ell_x \\ M_\psi \end{bmatrix} = \begin{bmatrix} A_1 & A_2 & A_3 \\ A_4 & A_5 & A_6 \\ A_7 & A_8 & A_9 \end{bmatrix} \begin{bmatrix} v_1 \\ v_2 \\ v_3 \end{bmatrix}, \quad (54)$$

where the elements A_i are given in the Appendix D and $\mathbf{v} = [v_1, v_2, v_3]^T$ is the new control input vector for the rotational dynamics in (19). This transformation yields the canonical form of the rotational dynamics of the UAV in (19).

Accordingly, our control laws for the 3D system will rely on a small displacement of the CM.

Step1. Altitude control and horizontal position: In this step, the control laws for T_1 (total thrust) and virtual control inputs u_x and u_y are formulated by using the same methodology of the 2D case. Following the Lyapunov methodology T_1 is obtained as follows:

$$T_1 = \frac{M}{\cos(x_5) \cos(x_9)} \left[g + e_3 + \ddot{x}_{3*} + k_3 e_4 - k_3^2 e_3 + k_4 e_4 \right], \quad (55)$$

Now, we have the solution for T_1 in the 3D case, similarly, we proceed by deriving the control laws for u_x and u_y responsible for the motion $x-y$ motion, yielding

$$u_x = \frac{M}{T_1} \left[e_7 + \ddot{x}_{7*} + k_7 e_8 - k_7^2 e_7 + k_8 e_8 \right], \quad (56)$$

where k_7 and k_8 are control gains. In (56), the error terms are defined as follows:

$$e_7 = x_{7*} - x_7 = x_* - x \quad (57)$$

$$e_8 = x_{8*} - x_8 = \dot{x}_* - \dot{x}. \quad (58)$$

$$u_y = \frac{M}{T_1} \left[e_1 + \ddot{x}_{1*} + k_5 e_2 - k_5^2 e_1 + k_6 e_2 \right], \quad (59)$$

The virtual control laws (56) and (59) determine the target pitch and roll angles which will be in turn used as target pitch and roll angles for the regulator of ℓ_y and ℓ_x . Now, the target pitch and roll angles are obtained from the virtual control inputs as:

$$x_{5*} = \phi_* = \sin^{-1} \left(\frac{u_x \sin(\psi_*) - u_y \cos(\psi_*)}{T_1} \right) \quad (60)$$

$$x_{9*} = \theta_* = \sin^{-1} \left(\frac{u_x \cos(\psi_*) - u_y \sin(\psi_*)}{T_1 \cos(x_{5*})} \right). \quad (61)$$

Step2. Pitch and roll angle control: Once we have set the target pitch ϕ_* and roll θ_* angles obtained through the virtual control laws u_x and u_y , the values of ℓ_y , and ℓ_x can be regulated. In detail,

$$v_1 = I_c \left[e_5 + k_1 e_6 - k_1^2 e_5 + k_2 e_6 \right],$$

$$v_2 = I_{cy} \left[e_9 + k_9 e_{10} - k_9^2 e_9 + k_{10} e_{10} \right],$$

where k_9 and k_{10} are control gains with positive value. $I_{yy} \approx I_{cy}$ is the approximated inertial term around the y axis. The error terms in (62) are defined as follows:

$$e_9 = x_{9*} - x_9 = \theta_* - \theta \quad (62)$$

$$e_{10} = x_{10*} - x_{10} = \dot{\theta}_* - \dot{\theta}. \quad (63)$$

Step3. Yaw control: The desired yaw angle ψ_* is then imposed so that the UAV heading and direction of motion follows the target path in the $x-y$ plane. From the illustration in Fig. 7 and trigonometry, the desired yaw angle ψ_* can be obtained as follows:

$$\psi_* = \tan^{-1} \left(\frac{y_* - y}{x_* - x} \right). \quad (64)$$

Proof. The proof of the derived control laws using the Lyapunov approach can be obtained similarly to the 2D case. In particular, for Step 1 the derivation follows the same procedure in Appendix A and B, while for Step 2 the one in Appendix C. Then, the control law in Step 3 follows straightforwardly. ■

TABLE II: Back-stepping controller tuning parameters

Parameter	k_1	k_2	k_3	k_4	k_5	k_6	ϵ_1
Linear trajectory	0.2	3	0.2	2	0.2	2	0.1
Complex trajectory	5	0.5	1	2	1.6	8	0.2

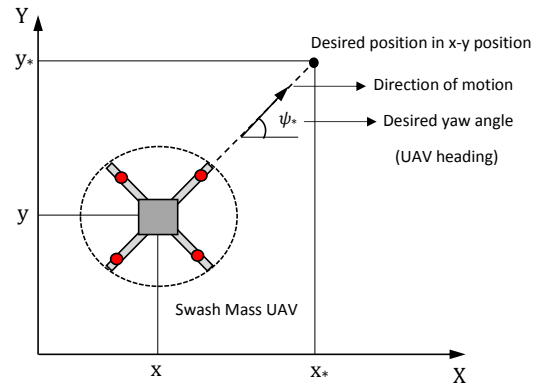


Fig. 7: Top view of the swash mass unmanned aerial vehicle structure, motion in $x-y$ plane.

VI. NUMERICAL RESULTS

In this section, numerical results are reported to evaluate the proposed control strategy for tracking given geometric trajectories to be followed by the UAV. Two flying scenarios are considered: a linear trajectory, and a complex trajectory. The total time of flight for both scenarios are set to $T_f = 10s$ and $T_f = 14s$, respectively, the sampling time is set to $T_s = 0.1ms$, and the initial conditions are $\mathbf{x}_{init} = [0, 0, 0, 0, 0, 0]^T$. For simplicity of exposition, the 2D planner case is shown. The value of the controller tuning parameters are reported in Table II.

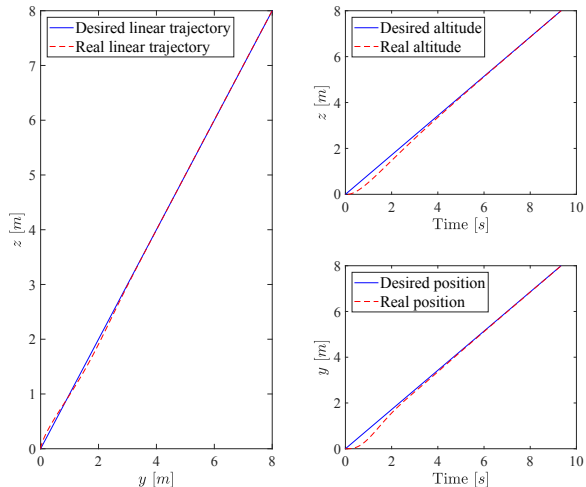


Fig. 8: Linear maneuver simulation.

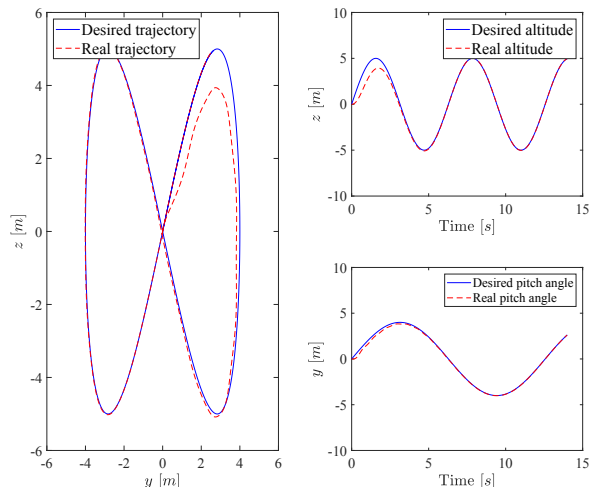
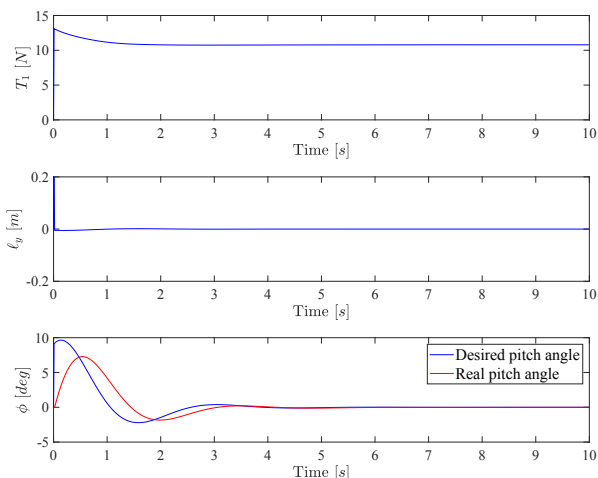


Fig. 10: Complex maneuver simulation.

Fig. 9: Control inputs $\mathbf{u} = [T_1, \ell_y]^T$ and pitch angle ϕ for the linear maneuver.

A. Linear Trajectory

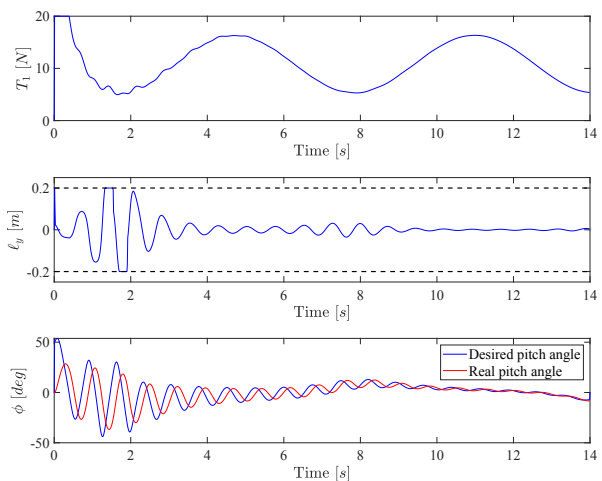
We start by considering a linear trajectory. In detail, this is given by

$$y_*(t) = x_{1*}(t) = 0.857t, \quad (65)$$

$$z_*(t) = x_{3*}(t) = 0.857t, \quad (66)$$

In Fig. 8, both the target and the real trajectories are shown and the difference is not pronounced. Quantitatively, in Table. III, we report the root-mean-square-error (RMSE) between the desired trajectory components and the real trajectory components. The overall RMSE is equal to $0.3m$.

The control inputs $\mathbf{u} = [T_1, \ell_y]^T$ are reported in Fig. 9. The target pitch angle obtained through the inverse of the virtual control input u_y is shown in the third sub-plot of Fig. 9. The actual (real) pitch angle of the UAV is also shown herein. The pitch angle oscillation is more pronounced at the beginning of the flight and then it converges to a constant value in steady state.

Fig. 11: Control inputs $\mathbf{u} = [T_1, \ell_y]^T$ and pitch angle ϕ for the complex trajectory.

B. Complex Trajectory

We now consider a complex trajectory given by the relations

$$y_*(t) = x_{1*}(t) = 4 \sin(0.5t), \quad (67)$$

$$z_*(t) = x_{3*}(t) = 5 \sin(t). \quad (68)$$

It simulates the behavior of the UAV in an aggressive maneuver, from a given orientation, upside down for the pitch angle ϕ , and a strong lateral motion y and altitude motion z . The results are reported in Fig. 10. Despite the aggressiveness of the trajectory, the UAV is able to well follow it. The real-target trajectory RMSE is reported in Table III and the overall RMSE equals $0.35m$.

TABLE III: Root-mean-square error between desired and real trajectory

Mission type	Value (m)
$RMSE_y$ for linear trajectory	0.2979
$RMSE_z$ for linear trajectory	0.3102
$RMSE_y$ for complex trajectory	0.1507
$RMSE_z$ for complex trajectory	0.5589

The control inputs for the complex trajectory are shown in Fig. 11. It is interesting to note that in the time window between 1s and 3s the control input ℓ_y is saturated to the value $\bar{\ell}_y = L = 0.2m$. Furthermore, the evolution of the control inputs follows a dumped sinusoidal shape, and this is directly related to the target motion trajectory in the $y-z$ plane.

VII. CONCLUSION

We have presented a new unmanned aerial vehicle (UAV) structure that allows maneuvering the UAV through the control of four swash masses and the double blade rotor thrust. A dynamical system model has been derived from the Newton's laws. It has been shown that a steady state can be defined and it corresponds to the state where the swash mass UAV is at rotation equilibrium and follows a linear trajectory. We have then focused the attention to the design of an automatic control mechanism so that the UAV follows a certain target trajectory. The dynamical system of equations that describes the UAV dynamics is non-linear and rather unique. In fact, it consists of sub-sets of differential equations coupled through the control inputs. Furthermore, the inertia term is time dependent as a result of the swash masses movement, which introduces a dependency on both the controllable masses positions and theirs derivative. A back-stepping control approach has then been derived considering physical constraints. Several results from simulations have been presented to assess the performance of the UAV that is maneuvered to follow both linear and aggressive trajectories. They show that the UAV can be controlled and such trajectories can be well followed with small RMSE.

APPENDIX A

DERIVATION OF THE CONTROL LAW FOR T_1

To derive the control law for T_1 , so that a target altitude is reached we start from equation (41) and follow the Lyapunov methodology [25] and ([19], Chapter 2), to identify a suitable Lyapunov candidate function. Firstly, the error term for the altitude $x_3 = z$ is defined

$$e_3 = x_{3*} - x_3. \quad (69)$$

A suitable candidate Lyapunov function is chosen as

$$V(e_3) = \frac{1}{2} \left(e_3^2 \right). \quad (70)$$

The first derivative of $V(e_3)$ with respect to time is given by

$$\dot{V}(e_3) = e_3 \dot{e}_3 = e_3 (\dot{x}_{3*} - \dot{x}_3). \quad (71)$$

If $x_4 = \dot{x}_{3*} + k_3 e_3$, for $k_3 > 0$, then $\dot{V}(e_3)$ is negative semi-definite and the error term e_3 converges to zero. Thus, x_{4*} is defined as

$$x_{4*} = \dot{x}_{3*} + k_3 e_3, \quad \text{for } k_3 > 0. \quad (72)$$

To get x_{4*} in (72), we should be able to control x_4 which comes from the dynamics equation defined in (38). Therefore, another error term e_4 can be defined

$$e_4 = x_{4*} - x_4 = \dot{x}_{3*} + k_3 e_3 - x_4. \quad (73)$$

Since we want both the error terms e_3 and e_4 to converge to zero, an augmented Lyapunov function of e_3 and e_4 is chosen:

$$V(e_3, e_4) = \frac{1}{2} \left(e_3^2 + e_4^2 \right). \quad (74)$$

By differentiating of $V(e_3, e_4)$ with respect to time, we obtain

$$\dot{V}(e_3, e_4) = e_3 \dot{e}_3 + e_4 \dot{e}_4. \quad (75)$$

Now, we need \dot{e}_3 and \dot{e}_4 so that they can be replaced into (75). If we differentiate (69) and considering (35), \dot{e}_3 is obtained:

$$\dot{e}_3 = \dot{x}_{3*} - \dot{x}_3 = \dot{x}_{3*} - x_4. \quad (76)$$

Then

$$\dot{e}_3 = e_4 - k_3 e_3. \quad (77)$$

Furthermore, by differentiating (73), \dot{e}_4 is obtained

$$\dot{e}_4 = \ddot{x}_{3*} + k_3 \dot{e}_3 - \dot{x}_4. \quad (78)$$

By replacing (77) and (78) into (75), $\dot{V}(e_3, e_4)$ results as

$$\dot{V}(e_3, e_4) = e_3 e_4 - k_3 e_3^2 + e_4 \ddot{x}_{3*} + k_3 \dot{e}_3 e_4 - e_4 \dot{x}_4. \quad (79)$$

In (79), \dot{x}_4 comes from the dynamical system defined in (37) and (38) and it can be replaced by the term $-g + \frac{\beta \Theta_2}{M} + \frac{T_1 \cos(x_5)}{M}$. The final form of $\dot{V}(e_3, e_4)$ is obtained as

$$\begin{aligned} \dot{V}(e_3, e_4) = & e_3 e_4 - k_3 e_3^2 + e_4 \ddot{x}_{3*} + k_3 e_4^2 \\ & - e_4 \left(-g + \frac{\beta \Theta_2}{M} + \frac{T_1 \cos(x_5)}{M} \right). \end{aligned} \quad (80)$$

In (80), T_1 represents the control force. By choosing T_1 properly, $\dot{V}(e_3, e_4)$ becomes negative semi-definite and the error terms e_3 and e_4 converge to zero. Thus, a suitable control law for T_1 is chosen as

$$T_1 = \frac{M}{\cos(x_5)} \left(g - \frac{\beta \Theta_2}{M} + e_3 + \ddot{x}_{3*} + k_3 e_4 - k_3^2 e_3 + k_4 e_4 \right), \quad (81)$$

where k_3 and k_4 are control gains with positive value. In fact, by substituting (52) in (51), $\dot{V}(e_3, e_4)$ becomes

$$\dot{V}(e_3, e_4) = -k_3 e_3^2 - k_4 e_4^2 < 0, \quad \text{for } k_3 > 0, \quad k_4 > 0. \quad (82)$$

Remark 5. In (81), the second order derivative of the desired altitude \ddot{x}_{3*} is added to the control law to increase the tracking performance.

APPENDIX B

DERIVATION OF THE CONTROL LAW FOR u_y

In this Appendix the virtual control input u_y is formulated to obtain a desired pitch angle $x_{5*} = \phi_*$. Following the Lyapunov methodology, let us consider the error term

$$e_1 = x_{1*} - x_1. \quad (83)$$

and consequently define the Lyapunov function

$$V(e_1) = \frac{1}{2} \left(e_1^2 \right). \quad (84)$$

We now compute its time derivative to obtain

$$\dot{V}(e_1) = e_1 \dot{e}_1 = e_1(\dot{x}_{1*} - \dot{x}_1). \quad (85)$$

If $x_2 = \dot{x}_{1*} + k_5 e_1$ for $k_5 > 0$, then $\dot{V}(e_1)$ is negative semi-definite and the error term e_1 converges to zero. To accomplish this we introduce

$$x_{2*} = \dot{x}_{1*} + k_5 e_1, \quad \text{for } k_5 > 0. \quad (86)$$

To get x_{2*} in (86), we should be able to control x_2 which comes from the dynamics given by (36). Therefore, another error term e_2 can be defined

$$e_2 = x_{2*} - x_2 = \dot{x}_{1*} + k_1 e_1 - x_2. \quad (87)$$

Now, we want both the error terms e_1 and e_2 to converge to zero. Therefore, an augmented Lyapunov function of e_1 and e_2 is chosen

$$V(e_1, e_2) = \frac{1}{2} \left(e_1^2 + e_2^2 \right). \quad (88)$$

By differentiating $V(e_1, e_2)$ with respect to the time, we obtain

$$\dot{V}(e_1, e_2) = e_1 \dot{e}_1 + e_2 \dot{e}_2. \quad (89)$$

After straightforward algebraic manipulations, we get

$$\dot{e}_1 = \dot{x}_{1*} - \dot{x}_1 = \dot{x}_{1*} - x_2, \quad (90)$$

then

$$\dot{e}_1 = e_2 - k_5 e_1. \quad (91)$$

Furthermore, by differentiating (87) with respect to time, \dot{e}_2 becomes

$$\dot{e}_2 = \ddot{x}_{1*} + k_5 \dot{e}_1 - \dot{x}_2. \quad (92)$$

By replacing (91) and (92) into (89), $\dot{V}(e_1, e_2)$ is obtained as follows

$$\dot{V}(e_1, e_2) = e_1 e_2 - k_5 e_1^2 + e_2 \ddot{x}_{1*} + k_5 \dot{e}_1 e_2 - e_2 \dot{x}_2. \quad (93)$$

In (93), \dot{x}_2 comes from the dynamical system of equations defined in (35) and (36). It can be replaced by the term $\frac{\beta \Theta_1}{M} + \frac{T_1 \sin(x_5)}{M}$. The final form of $\dot{V}(e_1, e_2)$ is obtained as

$$\begin{aligned} \dot{V}(e_1, e_2) = & e_1 e_2 - k_5 e_1^2 + e_2 \ddot{x}_{1*} + k_5 e_2^2 \\ & - e_2 \left(\frac{\beta \Theta_1}{M} + \frac{T_1 \sin(x_5)}{M} \right). \end{aligned} \quad (94)$$

In (94), $u_y = \sin(x_5)$ represents the virtual control input. By choosing u_y properly, $\dot{V}(e_1, e_2)$ becomes negative semi-definite so that the error terms e_1 and e_2 converge to zero. Thus, a suitable control law for u_y is chosen as

$$u_y = \frac{M}{T_1} \left(-\frac{\beta \Theta_1}{M} + e_1 + \ddot{x}_{1*} + k_5 e_2 - k_5^2 e_1 + k_6 e_2 \right), \quad (95)$$

where k_5 and k_6 are control gains with positive value. This is because, by substituting (95) in (94), $\dot{V}(e_1, e_2)$ becomes negative:

$$\dot{V}(e_1, e_2) = -k_1 e_1^2 - k_5 e_2^2 < 0, \quad \text{for } k_5 > 0, k_6 > 0. \quad (96)$$

APPENDIX C

DERIVATION OF THE CONTROL LAW FOR ℓ_y

The control law for ℓ_y is formulated in this Appendix following a similar methodology to the one used to derive the control laws for T_1 and u_y . Motivated by (39) and (40), the pitch tracking error is expressed as

$$e_5 = x_{5*} - x_5, \quad (97)$$

where x_{5*} represents the desired value for the pitch angle ϕ . We consider the Lyapunov candidate function

$$V(e_5) = \frac{1}{2} \left(e_5^2 \right). \quad (98)$$

Its time derivative is

$$\dot{V}(e_5) = e_5 \dot{e}_5 = e_5(\dot{x}_{5*} - \dot{x}_5). \quad (99)$$

By using the dynamical system equations in (39) and (40), we can replace \dot{x}_5 by x_6 and (99) becomes

$$\dot{V}(e_5) = e_5(\dot{x}_{5*} - x_6). \quad (100)$$

The stabilization of e_5 in (97) can be satisfied by introducing $x_6 = \dot{x}_{5*} + k_1 e_5$. Then $\dot{V}(e_5)$ is negative semi-definite for $k_1 > 0$. Because the fully actuated subsystem in (39) and (40) is a second order system we also want to stabilize the derivative of the pitch angle. Therefore, $x_{6*} = \dot{x}_{5*} + k_1 e_5$ for $k_1 > 0$. To stabilize the derivative of the pitch angle we need another error term which converges to zero. This error term is defined as follows

$$e_6 = x_{6*} - x_6. \quad (101)$$

To track x_{5*} and x_{6*} , the error terms e_5 and e_6 should converge to zero. We consider therefore the augmented Lyapunov function

$$V(e_5, e_6) = \frac{1}{2} \left(e_5^2 + e_6^2 \right). \quad (102)$$

The time derivative of (102) is

$$\dot{V}(e_5, e_6) = e_5 \dot{e}_5 + e_6 \dot{e}_6. \quad (103)$$

By taking (102) and $x_6 = \dot{x}_{5*} + k_1 e_5$ into account, e_6 is written as

$$e_6 = \dot{x}_{5*} + k_1 e_5 - x_6. \quad (104)$$

By replacing \dot{e}_5 with the term $(\dot{x}_{5*} - x_6)$ in (104), then e_6 becomes

$$e_6 = \dot{e}_5 + k_1 e_5. \quad (105)$$

By differentiating (105) with respect to time, \dot{e}_6 is obtained as

$$\dot{e}_6 = \ddot{x}_{5*} - \dot{x}_6 + k_1 \dot{e}_5. \quad (106)$$

By replacing (106) into (103), $\dot{V}(e_5, e_6)$ is given by

$$\dot{V}(e_5, e_6) = e_5(e_6 - k_1 e_5) + e_6(\ddot{x}_{5*} + k_1 \dot{e}_5 - \dot{x}_6). \quad (107)$$

In (107), \dot{x}_6 comes from the dynamical equations (39) and (40). By replacing \dot{x}_6 with $\frac{\beta T_1 \cos(x_5) \ell_y}{I_c}$ and with some simple calculations, finally we get

$$\begin{aligned} \dot{V}(e_5, e_6) = & e_5 e_6 - k_1 e_5^2 + \ddot{x}_{5*} e_6 + k_1 e_6^2 \\ & - k_1^2 e_5 e_6 - e_6 \left(\frac{\beta T_1 \cos(x_5) \ell_y}{I_c} \right). \end{aligned} \quad (108)$$

In (108), ℓ_y represents the control input. Now we should choose ℓ_y such that $\dot{V}(e_5, e_6)$ is negative semi-definite. Therefore, the control law of ℓ_y for the roll angle is chosen as

$$\ell_y = \frac{I_c}{\beta T_1 \cos(x_5)} \left(e_5 + k_1 e_6 - k_1^2 e_5 + k_2 e_6 \right), \quad (109)$$

where k_1 and k_2 are control gains with positive value. By substituting (109) into (108), $\dot{V}(e_5, e_6)$ becomes:

$$\dot{V}(e_5, e_6) = -k_1 e_5^2 - k_2 e_6^2 \quad \text{for } k_1 > 0, k_2 > 0 \quad (110)$$

We can conclude that if the control law of ℓ_y is chosen as (109), $\dot{V}(e_5, e_6)$ is negative semi-definite and the convergence of the error terms e_5 and e_6 to zero is fulfilled.

Remark 6. It should be observed that the errors \bar{e}_5 and \bar{e}_6 introduced in (51) and (52) converge asymptotically to zero since if we consider the Lyapunov function

$$V(\bar{e}_5, \bar{e}_6) = \frac{1}{2} \left(\bar{e}_5^2 + \bar{e}_6^2 \right), \quad (111)$$

by substituting (53) and (50) to its derivative,

$$\dot{V}(\bar{e}_5, \bar{e}_6) = -k_1 \bar{e}_5^2 - k_2 \bar{e}_6^2, \quad (112)$$

this is negative for all positive parameters k_1 and k_2 . Consequently, since also the auxiliary error goes to zero, the pitch angle error is also asymptotically null.

APPENDIX D

THE DECOUPLING MATRIX

The elements $A_i, i = 1, \dots, 9$, in (54) are

$$\begin{aligned} A_1 &= \cos(\phi) \sin(\psi) - \cos(\psi) \sin(\phi) \sin(\theta) \\ A_2 &= \cos(\psi) \cos(\theta) \\ A_3 &= \sin(\phi) \sin(\psi) + \cos(\phi) \cos(\psi) \sin(\theta) \\ A_4 &= \cos(\phi) \cos(\psi) + \sin(\phi) \sin(\psi) \cos(\theta) \\ A_5 &= \cos(\theta) \sin(\psi) \\ A_6 &= -\cos(\psi) \sin(\phi) + \cos(\phi) \sin(\psi) \sin(\theta) \\ A_7 &= \cos(\theta) \sin(\phi) \\ A_8 &= \sin(\theta) \\ A_9 &= \cos(\phi) \cos(\theta). \end{aligned}$$

REFERENCES

- [1] R. Austin, *Unmanned Aircraft Systems: UAVs Design, Development and Deployment*, ser. AIAA education series. American Institute of Aeronautics and Astronautics, 2010.
- [2] D. Brescianini and R. D'Andrea, "Design, modeling and control of an omni-directional aerial vehicle," in *2016 IEEE International Conference on Robotics and Automation (ICRA)*, May 2016, pp. 3261–3266.
- [3] M. Zamani, J. Trumpf, and R. Mahony, "Minimum-energy filtering for attitude estimation," *IEEE Transactions on Automatic Control*, vol. 58, no. 11, pp. 2917–2921, Nov 2013.
- [4] C. Papachristos, K. Alexis, and A. Tzes, "Efficient force exertion for aerial robotic manipulation: Exploiting the thrust-vectoring authority of a tri-tiltrotor uav," in *2014 IEEE International Conference on Robotics and Automation (ICRA)*, May 2014, pp. 4500–4505.
- [5] Y. Long and D. J. Cappelleri, *Omnicopter: A Novel Overactuated Micro Aerial Vehicle*. Heidelberg: Springer International Publishing, 2013, pp. 215–226.
- [6] M. Ryll, H. H. Blthoff, and P. R. Giordano, "A novel overactuated quadrotor unmanned aerial vehicle: Modeling, control, and experimental validation," *IEEE Transactions on Control Systems Technology*, vol. 23, no. 2, pp. 540–556, March 2015.
- [7] P. C. Garcia, R. Lozano, and A. E. Dzul, *Modelling and Control of Mini-Flying Machines*, 1st ed. Springer Publishing Company, Incorporated, 2010.
- [8] B. Salamat and A. M. Tonello, "Novel trajectory generation and adaptive evolutionary feedback controller for quadrotors," in *2018 IEEE Aerospace Conference*, March 2018, pp. 1–8.
- [9] M. Faessler, D. Falanga, and D. Scaramuzza, "Thrust mixing, saturation, and body-rate control for accurate aggressive quadrotor flight," *IEEE Robotics and Automation Letters*, vol. 2, no. 2, pp. 476–482, April 2017.
- [10] M. Weiss and T. Shima, "Linear quadratic optimal control-based missile guidance law with obstacle avoidance," *IEEE Transactions on Aerospace and Electronic Systems*, vol. 55, no. 1, pp. 205–214, Feb 2019.
- [11] A. Gruszka, M. Malisoff, and F. Mazenc, "Bounded tracking controllers and robustness analysis for UAVs," *IEEE Transactions on Automatic Control*, vol. 58, no. 1, pp. 180–187, Jan 2013.
- [12] R. P. Anderson and D. Milutinovi, "A stochastic approach to dubins vehicle tracking problems," *IEEE Transactions on Automatic Control*, vol. 59, no. 10, pp. 2801–2806, Oct 2014.
- [13] S. R. Arya, S. Rao, and B. Dattaguru, "Effect of asymmetric control constraints on fixed-wing uav trajectories," *IEEE Transactions on Aerospace and Electronic Systems*, pp. 1–1, 2018.
- [14] J. A. Acosta, R. Ortega, A. Astolfi, and A. D. Mahindrakar, "Interconnection and damping assignment passivity-based control of mechanical systems with underactuation degree one," *IEEE Transactions on Automatic Control*, vol. 50, no. 12, pp. 1936–1955, Dec 2005.
- [15] R. Ortega, M. W. Spong, F. Gomez-Estern, and G. Blankenstein, "Stabilization of a class of underactuated mechanical systems via interconnection and damping assignment," *IEEE Transactions on Automatic Control*, vol. 47, no. 8, pp. 1218–1233, Aug 2002.
- [16] A. P. Aguiar and J. P. Hespanha, "Trajectory-tracking and path-following of underactuated autonomous vehicles with parametric modeling uncertainty," *IEEE Transactions on Automatic Control*, vol. 52, no. 8, pp. 1362–1379, Aug 2007.
- [17] H. Sun, L. Hou, G. Zong, and X. Yu, "Fixed-time attitude tracking control for spacecraft with input quantization," *IEEE Transactions on Aerospace and Electronic Systems*, vol. 55, no. 1, pp. 124–134, Feb 2019.
- [18] J. Watkinson, *Art of the Helicopter*. Elsevier Science, 2003.
- [19] J. Zhou and C. Wen, *Adaptive Backstepping Control of Uncertain Systems: Nonsmooth Nonlinearities, Interactions or Time-Variations*. Springer Berlin Heidelberg, 2008.
- [20] B. Etkin, *Dynamics of Atmospheric Flight*. Courier Corporation, 2012.
- [21] A. A. Shabana, *Dynamics of Multibody Systems*. Cambridge University Press, 2005.
- [22] S. Rosati, *Fisica generale*, C. E. Ambrosiana-Milano, Ed., 1978.
- [23] H. Goldstein, C. Poole, and J. Safko, *Classical Mechanics*. Addison Wesley, 2002.
- [24] T. Madani and A. Benallegue, "Backstepping control for a quadrotor helicopter," in *2006 IEEE/RSJ International Conference on Intelligent Robots and Systems*, Oct 2006, pp. 3255–3260.
- [25] H. K. Khalil, *Nonlinear systems; 3rd ed.* Upper Saddle River, NJ: Prentice-Hall, 2002.
- [26] E. P. Anderson, R. W. Beard, and T. W. McLain, "Real-time dynamic trajectory smoothing for unmanned air vehicles," *IEEE Transactions on Control Systems Technology*, vol. 13, no. 3, pp. 471–477, May 2005.
- [27] B. Salamat and A. M. Tonello, "Stochastic trajectory generation using particle swarm optimization for quadrotor unmanned aerial vehicles (UAVs)," *Aerospace*, vol. 4, no. 2, 2017.
- [28] B. Salamat and A. M. Tonello, "A generalized multi-objective framework for UAV mission planning," in *2019 IEEE Aerospace Conference*, March 2019.
- [29] H. Chen, K. Chang, and C. S. Agate, "Uav path planning with tangent-plus-lyapunov vector field guidance and obstacle avoidance," *IEEE Transactions on Aerospace and Electronic Systems*, vol. 49, no. 2, pp. 840–856, APRIL 2013.
- [30] S. Sastry, *Nonlinear Systems: Analysis, Stability, and Control*, ser. Interdisciplinary Applied Mathematics. Springer New York, 1999.